ELSEVIER

Nuclear Physics B 601 (2001) 3–23

NUCLEAR PHYSICS B

www.elsevier.nl/locate/npe

Inclusive production of $\rho^0(770)$, $f_0(980)$ and $f_2(1270)$ mesons in ν_μ charged current interactions

NOMAD Collaboration

P. Astier [n], D. Autiero [h], A. Baldisseri [r], M. Baldo-Ceolin [m], M. Banner [n], G. Bassompierre [a], K. Benslama [i], N. Besson [r], I. Bird [h,i], B. Blumenfeld [b], F. Bobisut [m], J. Bouchez [r], S. Boyd [t], A. Bueno [c,x], S. Bunyatov [f], L. Camilleri [h], A. Cardini [j], P.W. Cattaneo [o], V. Cavasinni [p], A. Cervera-Villanueva [h,v], G. Collazuol [m], G. Conforto [u], C. Conta [o], M. Contalbrigo [m], R. Cousins [j], D. Daniels [c], H. Degaudenzi [i], T. Del Prete [p], A. De Santo [h], T. Dignan [c], L. Di Lella [h], E. do Couto e Silva [h], J. Dumarchez [n], M. Ellis [t], T. Fazio [a], G.J. Feldman [c], R. Ferrari [o], D. Ferrère [h], V. Flaminio [p], M. Fraternali [o], J.-M. Gaillard [a], E. Gangler [h,n], A. Geiser [e,h], D. Geppert [e], D. Gibin [m], S. Gninenko [h,l], A. Godley [t], J.-J. Gomez-Cadenas [h,v], J. Gosset [r], C. Gößling [e], M. Gouanère [a], A. Grant [h], G. Graziani [g], A. Guglielmi [m], C. Hagner [r], J. Hernando [v], D. Hubbard [c], P. Hurst [c], N. Hyett [k], E. Iacopini [g], C. Joseph [i], F. Juget [i], M. Kirsanov [l], O. Klimov [f], J. Kokkonen [h], A. Kovzelev [l,o], A. Krasnoperov [a,f], V. Kuznetsov [f,h], S. Lacaprara [m], C. Lachaud [n], B. Lakić [w], A. Lanza [o], L. LaRotonda [d], M. Laveder [m], A. Letessier-Selvon [n], J.-M. Levy [n], L. Linssen [h], A. Ljubičić [w], J. Long [b], A. Lupi [g], A. Marchionni [g], F. Martelli [u], X. Méchain [r], J.-P. Mendiburu [a], J.-P. Meyer [r], M. Mezzetto [m], S.R. Mishra [c,s], G.F. Moorhead [k], D. Naumov [f], P. Nédélec [a], Yu. Nefedov [f], C. Nguyen-Mau [i], D. Orestano [q], F. Pastore [q], L.S. Peak [t], E. Pennacchio [u], H. Pessard [a], R. Petti [h,o], A. Placci [h], G. Polesello [o], D. Pollmann [e], A. Polyarush [l], B. Popov [f,n], C. Poulsen [k], P. Rathouit [r], J. Rico [x], C. Roda [h,p], A. Rubbia [h,x], F. Salvatore [o], K. Schahmaneche [n], B. Schmidt [e,h], M. Sevior [k], D. Sillou [a], F.J.P. Soler [h,t], G. Sozzi [i], D. Steele [b,i], U. Stiegler [h], M. Stipčević [w], Th. Stolarczyk [r], M. Tareb-Reyes [i], G.N. Taylor [k], V. Tereshchenko [f], A. Toropin [l], A.-M. Touchard [n], S.N. Tovey [k], M.-T. Tran [i], E. Tsesmelis [h], J. Ulrichs [t], L. Vacavant [i], M. Valdata-Nappi [d,1], V. Valuev [f,j], F. Vannucci [n],

0550-3213/01/$ – see front matter
PII: S0550-3213(01)00054-2

RAPID COMMUNICATION

K.E. Varvell [t], M. Veltri [u], V. Vercesi [o], G. Vidal-Sitjes [h,v], J.-M. Vieira [i], T. Vinogradova [j], F.V. Weber [c,h], T. Weisse [e], F.F. Wilson [h], L.J. Winton [k], B.D. Yabsley [t], H. Zaccone [r], K. Zuber [e], P. Zuccon [m]

[a] *LAPP, Annecy, France*
[b] *Johns Hopkins University, Baltimore, MD, USA*
[c] *Harvard University, Cambridge, MA, USA*
[d] *University of Calabria and INFN, Cosenza, Italy*
[e] *Dortmund Universität, Dortmund, Germany*
[f] *JINR, Dubna, Russia*
[g] *University of Florence and INFN, Florence, Italy*
[h] *CERN, Geneva, Switzerland*
[i] *University of Lausanne, Lausanne, Switzerland*
[j] *UCLA, Los Angeles, CA, USA*
[k] *University of Melbourne, Melbourne, Australia*
[l] *Institute Nucl. Research, INR Moscow, Russia*
[m] *University of Padova and INFN, Padova, Italy*
[n] *LPNHE, University of Paris VI and VII, Paris, France*
[o] *University of Pavia and INFN, Pavia, Italy*
[p] *University of Pisa and INFN, Pisa, Italy*
[q] *Roma Tre University and INFN, Rome, Italy*
[r] *DAPNIA, CEA Saclay, France*
[s] *University of South Carolina, Columbia, SC, USA*
[t] *University of Sydney, Sydney, Australia*
[u] *University of Urbino, Urbino, and INFN Florence, Italy*
[v] *IFIC, Valencia, Spain*
[w] *Rudjer Bošković Institute, Zagreb, Croatia*
[x] *ETH Zürich, Zürich, Switzerland*

Received 21 December 2000; accepted 22 January 2001

Abstract

The inclusive production of the meson resonances $\rho^0(770)$, $f_0(980)$ and $f_2(1270)$ in neutrino–nucleus charged current interactions has been studied with the NOMAD detector exposed to the wide band neutrino beam generated by 450 GeV protons at the CERN SPS. For the first time the $f_0(980)$ meson is observed in neutrino interactions. The statistical significance of its observation is 6 standard deviations. The presence of $f_2(1270)$ in neutrino interactions is reliably established. The average multiplicity of these three resonances is measured as a function of several kinematic variables. The experimental results are compared to the multiplicities obtained from a simulation based on the Lund model. In addition, the average multiplicity of $\rho^0(770)$ in antineutrino–nucleus interactions is measured.

Keywords: Inclusive; Resonance production; Neutrino interactions

E-mail address: mikhail.kirsanov@cern.ch (M. Kirsanov).
[1] Now at University of Perugia and INFN, Perugia, Italy.

1. Introduction

Hadron production in high energy neutrino–nucleon charged current (CC) interactions can be represented as a two-step process. The first step is the interaction of a W boson with a quark of the target nucleon changing it into a quark of a different flavour. The second step is the hadronization of the quarks during which coloured partons fragment into colourless hadrons. Perturbative QCD not being applicable to the soft process of hadronization, phenomenological models must be used. The most successful models are the string [1] and cluster fragmentation [2] models.

A significant fraction of the particles in the hadron jets directly observed are produced through the production and decay of a large variety of very short lived particles, the so-called resonances. Consequently, the study of inclusive meson and baryon resonances is believed to reveal more directly the primary interaction mechanism than the studies of stable particles (such as pions and kaons). Therefore, resonance production provides a better ground for comparisons between models and experimental results. Inclusive resonance production has been extensively studied in e^+e^- annihilation [3–8], photoproduction [9], electroproduction by muons [10], in hadronic interactions [11].

The role of the orbitally excited mesons, for example $f_0(980)(J^{PC} = 0^{++})$ and $f_2(1270)(J^{PC} = 2^{++})$, is of special interest in view of the possibly different production mechanisms. Both mesons have an orbital angular momentum equal to 1 and a sum of spins of the valence quarks also equal to 1 resulting in a total spin of 0 for the $f_0(980)$ and of 2 for the $f_2(1270)$.

A number of nonstandard interpretations of the $f_0(980)$ state have been suggested. One approach regards the $f_0(980)$ as a four quark bound state [12], another as a two-kaon molecule [13]. Gribov [14] has proposed a new theory of QCD confinement, in which the $f_0(980)$ plays the special role of a novel vacuum scalar state. Close et al. [15] noticed that the signature of Gribov's vacuum scalar state would be an enhanced yield in low multiplicity events. Robson [16] proposed an interpretation of the $f_0(980)$ as a scalar glueball. A recent OPAL study of the $f_0(980)$ at LEP [4] does not confirm the Gribov interpretation. All measured characteristics of $f_0(980)$ production in Z^0 decays are consistent with the $f_0(980)$ being a conventional scalar meson. However, an analysis of the WA102 data by Close and Kirk [17] selects the 'enigmatic' $f_0(980)$ as a glueball candidate together with $f_0(1500)$, $f_J(1710)$ and $f_2(1900)$.

Bubble chambers used to be the only detectors where inclusive production of ρ and other resonances in neutrino interactions could be studied. In such detectors detailed information about the final state particles in each event can be obtained. The neutrino experiments [18–30] studied inclusive production of $\rho^0(770)$ and, in some cases, of $f_2(1270)$ resonances. BEBC WA59 [20] studied $\rho(770)$ (all three charge states), $\eta(550)$, $\omega(783)$ and $f_2(1270)$. The resonance production properties were measured as a function of the mass of the hadronic system, of the charged hadron multiplicity and of various other kinematical variables.

The main problem common to these studies was the small statistics (the total of all experiments amounts to about 60 000 ν_μ CC events). The level of accuracy corresponding

to this statistics did not necessitate taking into account the reflections of other resonances (for the definition of reflections see Section 5). They were not accounted for in most of the previous neutrino experiments. Due to low statistics there were no attempts to look for the $f_0(980)$ meson in neutrino data. As to the other orbitally excited meson, BEBC WA21 [19] using 17750 ν_μp interactions found 615 ± 226 $f_2(1270)$ mesons. But later, in the combined WA21 + WA25 + WA59 + E180 [31] data sample (58866 ν_μ CC events), no observation of $f_2(1270)$ was reported.

All previous experiments reported an overestimation of the average multiplicities of $\rho^0(770)$ by the Lund model by 50–70%, while the shapes of the Lund distributions were in agreement with the experimental distributions.

The NOMAD experiment in 4 years of data taking (1995–1998) has collected about $1.3 \times 10^6 \nu_\mu$ CC interactions. In addition, a short antineutrino run has provided about 32 000 $\bar{\nu}_\mu$ CC events. The large statistics of the NOMAD data and the good quality of the event reconstruction make possible the study of processes that could not be studied in previous neutrino experiments.

The article is organized as follows: Section 2 describes the experimental setup including the NOMAD detector, the neutrino beam and the NOMAD simulation software; in Section 3 the kinematical variables used in this analysis are defined; Section 4 and Section 5 describe the details of the analysis; the results are presented and discussed in Section 6; Section 7 is devoted to the systematic uncertainties; the multiplicities measured in this analysis are compared with the results of previous experiments in Section 8; summary and conclusions are given in Section 9.

2. The experimental setup

2.1. The NOMAD detector

The NOMAD detector (see Fig. 1) has been described in details elsewhere [32]. It consists of a number of sub-detectors most of which are located inside a 0.4 T dipole magnet with an inner volume of $7.5 \times 3.5 \times 3.5$ m^3: an active target made of drift chambers (DC) [33] with a mass of 2.7 tons, an average density of 0.1 g/cm^3 and a total length of about one radiation length ($\sim 1.0 X_0$), followed by a transition radiation detector (TRD) [34], a preshower detector and an electromagnetic calorimeter (ECAL) consisting of 875 lead glass cells [35]. The low density and the good instrumentation of the active target (there is less than 1% of a radiation length between two consecutive measurements) allow to obtain detailed information about the final state of neutrino interactions. The momentum resolution for reconstructed tracks is, on average, 3.5% for momenta below 20 GeV/c [32], relevant to most of the final state hadrons.

The TRD is used for electron identification. It provides a pion rejection factor greater than 10^3 for a 90% electron efficiency in the momentum range from 1 GeV/c to 50 GeV/c.

The ECAL provides an energy resolution of $3.2\%/\sqrt{E\ [\mathrm{GeV}]} \oplus 1\%$ for electromagnetic showers and is essential to measure the total energy flow in neutrino interactions. The preshower detector is used for electron and gamma identification.

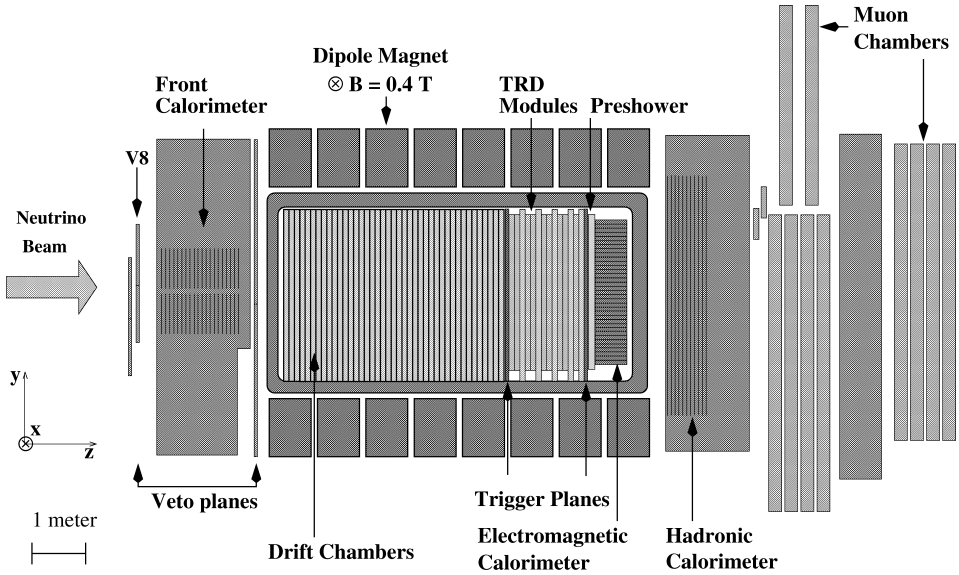

Fig. 1. Side view of the NOMAD detector. The origin of the coordinate system is on the upstream face of the active target.

A hadron calorimeter is located just after the magnet coil. It is followed by an iron absorber and a set of muon chambers. The muon identification efficiency is 97% for muons of momentum higher than 5 GeV/c.

The neutrino interaction trigger [36] consists of a coincidence between signals from two planes of counters located after the active target in the absence of a signal from a large area system of veto counters located upstream of the NOMAD detector.

The NOMAD target consists mainly of carbon (on which about 80% of the ν_μ CC interactions occur) and of other elements with similar atomic numbers (mostly oxygen and nitrogen).

2.2. The neutrino beam

The NOMAD detector is located in the WANF neutrino beam line [37] at CERN. In the main focusing mode (positive focusing) the beam is an essentially pure ν_μ beam (about 93%). In negative focusing it is mainly a $\bar{\nu}_\mu$ beam of lower purity (about 71%). More details about the beam composition can be found in Table 1 [38] and Table 2.

2.3. The Monte Carlo simulations

In this analysis the Monte Carlo (MC) simulation software is based on the LEPTO6.1 [39]–JETSET7.4 [40] event generator and a full GEANT321 [41] detector simulation.

The simulated events passed through the same reconstruction program and selection criteria that were used for the data.

Table 1
The CERN SPS neutrino beam composition in the positive focusing mode

Neutrino	Flux		CC interactions in NOMAD	
flavours	$\langle E_\nu \rangle$ [GeV]	Rel. abund.	$\langle E_\nu \rangle$ [GeV]	Rel. abund.
ν_μ	23.5	1	43.8	1
$\bar{\nu}_\mu$	19.2	0.0612	42.8	0.0255
ν_e	37.1	0.0094	58.3	0.0148
$\bar{\nu}_e$	31.3	0.0024	54.5	0.0016

Table 2
The CERN SPS neutrino beam composition in the negative focusing mode

Neutrino	Flux		CC interactions in NOMAD	
flavours	$\langle E_\nu \rangle$ [GeV]	Rel. abund.	$\langle E_\nu \rangle$ [GeV]	Rel. abund.
ν_μ	23.5	0.156	58	0.383
$\bar{\nu}_\mu$	19.6	1	33.9	1
ν_e	31.1	0.0053	56.3	0.016
$\bar{\nu}_e$	29.5	0.0086	47.8	0.013

An important JETSET parameter for the fragmentation, the fragmentation cutoff,[2] was set to 0.2 GeV. The strangeness suppression factor[3] was set to 0.21. These values were obtained from a study of hadronic states [42] with invariant masses similar to those studied in this analysis. This was also checked by comparing the fragmentation function of pions and K^0_S obtained from the MC with the one obtained from the NOMAD data.

In order to generate $f_0(980)$ and $f_2(1270)$ with rates comparable to those observed in our data we changed the default values of the following JETSET parameters (the default values for both parameters in JETSET7.4 is zero): the probability[4] to produce mesons with orbital angular momentum 1 and total angular momentum 0 equal to 0.08; the probability[5] to produce mesons with orbital angular momentum 1 and total angular momentum 2 equal to 0.185. Note that setting these parameters different from zero decreases the number of $\rho^0(770)$ mesons in the MC by the sum of values given above (in our case by 26.5%).

The MC includes a simulation of nuclear effects [43] which takes into account the rescattering and absorption of particles inside nuclei. This allowed us to deconvolute these effects from our results and extract the resonance yields on free nucleons. At our energies and target composition these effects are small.

[2] PARJ(33) in JETSET7.4.
[3] PARJ(2) in JETSET7.4.
[4] PARJ(15) in JETSET7.4.
[5] PARJ(17) in JETSET7.4.

The Monte Carlo allows for a direct test of the fitting procedure used to extract the number of resonances from the invariant mass plots since the number of simulated $\rho^0(770)$ mesons is known. In addition, systematic effects due to other resonances can be studied since for most of the reconstructed tracks it is possible to match a MC particle at the level of the event generator.

3. Definition of the kinematical variables

The following variables are used in this analysis:

1. The global event variables:
   - E_{vis} — the total visible energy of the event calculated as the sum of the energies of all tracks assigned to the primary vertex and of ECAL clusters identified as photons. The reconstructed charged particles were assigned the mass of the pion except for identified muons and electrons which were assigned their respective masses;
   - ΔE_{vis} — the measurement error on E_{vis}, calculated from the uncertainty on the fitted momentum for each track and from the known energy resolution of the ECAL;
   - P_t^{miss} — the modulus of the transverse component of the total event momentum with respect to the neutrino beam direction. Lost and mismeasured particles are the main contributors to the value of P_t^{miss};
   - E_ν — the neutrino energy in the laboratory system. Monte Carlo studies show that the reconstructed hadronic energy is, on the average, underestimated, and that this underestimate is correlated with P_t^{miss}. We have therefore corrected E_{vis} by adding a term depending on P_t^{miss} and the hadronic energy. E_ν is determined with a resolution of about 10% and with a systematic error not exceeding 1% in the whole energy range of interest;
   - $\nu = E_\nu - E_\mu$, where E_μ is the energy of the track identified as a muon: energy transfer from the neutrino to the hadrons in the laboratory system. If there were more than one muon candidate, the one with the greater transverse momentum was chosen;
   - $q = p_\nu - p_\mu$ — the 4-momentum transfer;
   - $Q^2 = -q^2$ — the 4-momentum transfer squared;
   - $W^2 = m_N^2 + 2m_N\nu - Q^2$ — the hadronic invariant mass squared (m_N is the nucleon mass).
2. The resonance candidate variables:
   - $x_F = 2p_\parallel / W$ ($p_\parallel$ is the longitudinal momentum of the resonance candidate in the rest frame of the hadronic system) — Feynman x variable;
   - $z = E/\nu$ (where E is the energy of the resonance candidate) — fragmentation function variable;
   - $p_\perp$ — modulus of the transverse momentum of the resonance candidate relative to the total momentum of the hadron jet.

4. Data sample and event selection

The present analysis is based on the full NOMAD data sample. For the ν_μ analysis we used the data taken with the neutrino beam set to positive focusing. A study of $\bar{\nu}_\mu$ in the positive focusing mode would require additional cuts to reduce the admixture of misidentified ν_μ, which could render a comparison with other experiments difficult. For this reason, for the $\bar{\nu}_\mu$ study only the negative focusing mode was used.

A $\nu_\mu(\bar{\nu}_\mu)$ CC event was selected for further processing if:

- there was an identified $\mu^-(\mu^+)$ at the primary vertex with momentum $p_\mu > 3$ GeV/c (this cut ensures a good muon identification and a consistency with previous neutrino experiments);
- the invariant mass of the hadronic system W was higher than 2 GeV (in order to limit the study to the deep inelastic region);
- there were at least 3 tracks (including the muon) at the primary vertex (this is necessary to build a resonance candidate).

The following quality cuts were applied in order to ensure an accurate event reconstruction:

- the primary vertex (see Fig. 1 for the coordinate system) should be inside the following fiducial volume:

$$|X, Y| < 120 \text{ cm}, \qquad 10 \text{ cm} < Z < 390 \text{ cm};$$

- the event should be measured with reasonable accuracy ($\Delta E_{\text{vis}}/E_{\text{vis}} < 30\%$).

After cuts we obtain 669252 ν_μ CC and 15927 $\bar{\nu}_\mu$ CC event candidates.

5. Extraction of the resonance signal

All combinations of tracks with momenta larger than 0.1 GeV/c originating at the primary vertex and not identified as electrons or muons were used for the construction of the resonance candidates. All used tracks were assigned the pion mass.

The distribution of the $\pi^+\pi^-$ invariant mass is shown in Fig. 2. For comparison the distribution of the invariant mass of $\pi^+\pi^+$ and $\pi^-\pi^-$ pairs is shown in Fig. 3. The $\pi^+\pi^-$ distribution shows an enhancement at the $\rho^0(770)$ mass which is not present in the like-sign distribution. When a cut $x_F > 0.6$ is applied to reduce the combinatorial background, clear peaks at the $f_0(980)$ and $f_2(1270)$ masses become visible, as shown in Fig. 4.

We now address the treatment of reflections. Reflections are contributions to the $\pi^+\pi^-$ invariant mass distribution from resonances decaying to $\pi^+\pi^-$ + some other particles (e.g., $\omega \to \pi^+\pi^-\pi^0$) or contributions from resonances decaying to particles other than pions and thus assigned wrong mass values. The reflections were estimated from the fully simulated MC events and taken into account in the fit of the $\pi^+\pi^-$ invariant mass distribution (Fig. 5). It is possible however that the multiplicity of the resonances giving reflections in the data could be different from the one in the MC. In order to take this into account the sum of all reflections obtained from the MC was multiplied by an overall

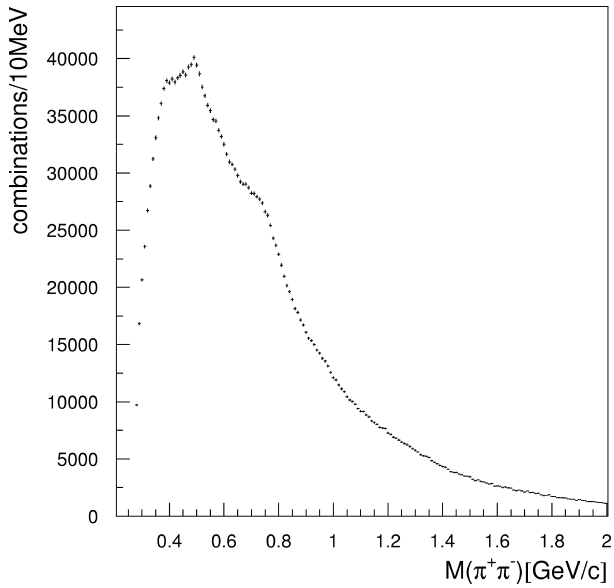

Fig. 2. Raw distribution of the $\pi^+\pi^-$ invariant mass in the ν_μ CC sample.

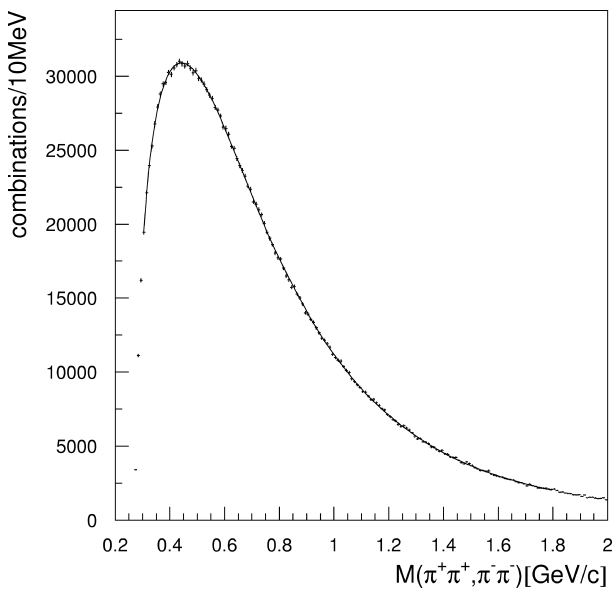

Fig. 3. Raw distribution of the invariant mass of $\pi^+\pi^+$ and $\pi^-\pi^-$ pairs in the ν_μ CC sample. The line is the result of the fit described in the text.

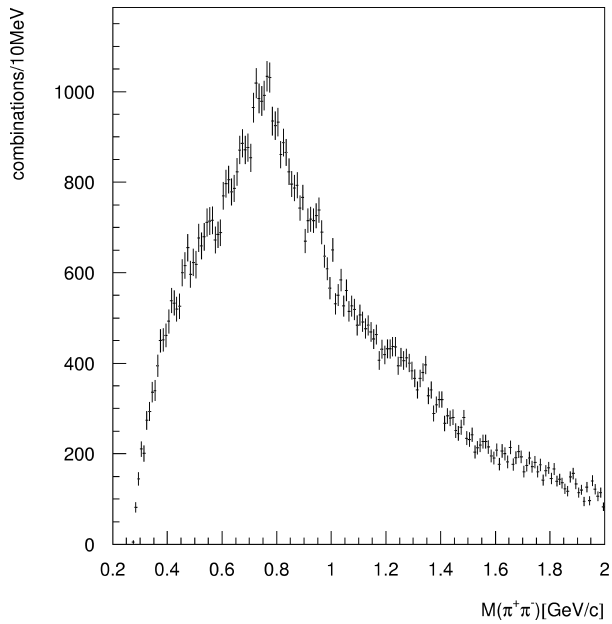

Fig. 4. Raw distribution of the $\pi^+\pi^-$ invariant mass with $x_F > 0.6$.

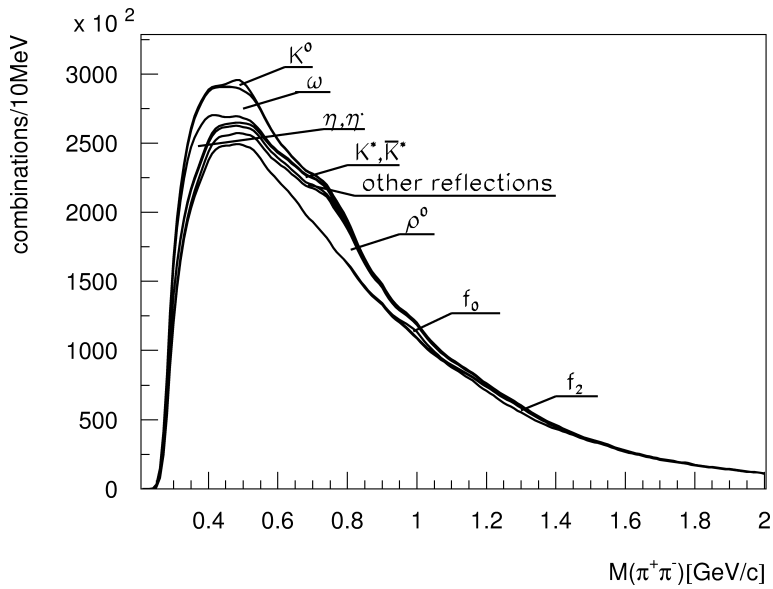

Fig. 5. $\pi^+\pi^-$ invariant mass distribution of Monte Carlo events including the contributions of signal, reflections and combinatorial background.

normalization factor p which was left as a free parameter in the fit. In NOMAD an additional contribution to the $\pi^+\pi^-$ invariant mass distribution arises from early decays of K^0_S and misidentified γ conversions (see Fig. 5). For distances less than 15 cm from the primary vertex along the beam axis it is difficult to distinguish tracks beginning at the primary vertex from tracks originating at a V^0 vertex. This contribution was also estimated from the MC simulation and taken into account together with other reflections. As can be seen in Fig. 5, the largest contribution is from $\omega \to \pi^+\pi^-\pi^0$.

Ignoring reflections could result in incorrect determination of the resonance parameters. As an example, in our case this would result in a ρ^0 mass value extracted from the fit about 10 MeV lower than the accepted value [44].

The resonance signal is determined by fitting the invariant mass distribution of all possible $\pi^+\pi^-$ combinations, dN/dm, to the expression

$$\frac{dN}{dm} = \big[1 + \mathrm{BW}(m)\big]\mathrm{BG}(m) + p \cdot \mathrm{RF}(m), \tag{1}$$

where

$$\mathrm{BW}(m) = a_1\mathrm{BW}_\rho(m) + a_2\mathrm{BW}_{f_0}(m) + a_3\mathrm{BW}_{f_2}(m), \tag{2}$$

is a relativistic Breit–Wigner function [45], $\mathrm{BG}(m)$ is the combinatorial background and $\mathrm{RF}(m)$ is the contribution from reflections.

The Breit–Wigner function is

$$\mathrm{BW} = \frac{m}{k}\frac{m_\mathrm{R}\Gamma'_\mathrm{R}}{(m^2 - m_\mathrm{R}^2)^2 + m_\mathrm{R}^2\Gamma'^2_\mathrm{R}}, \tag{3}$$

where

$$\Gamma'_\mathrm{R} = \Gamma_\mathrm{R}\left(\frac{k}{k_\mathrm{R}}\right)^{2L+1}\frac{m_\mathrm{R}}{m}. \tag{4}$$

Here m_R and Γ_R are the mass and width of the resonance R; L is the relative orbital angular momentum of the two pions (equal to the spin of the resonance): $L = 0$ for $f_0(980)$, $L = 1$ for $\rho^0(770)$, and $L = 2$ for $f_2(1270)$; k is the pion momentum in the resonance rest frame; k_R is the value of k when $m = m_\mathrm{R}$.

The background was assumed to have the following shape

$$\mathrm{BG} = a_4(m - 2m_\pi)^{a_5}\exp\big(a_6 m + a_7 m^2 + a_8 m^3\big), \tag{5}$$

which takes into account the threshold effect and the exponential fall-off of the distribution at high values of m.

In Eq. (1) the Breit–Wigner functions are multiplied by BG in order to account for the available phase-space. The parameters a_1 to a_8, p and the masses and widths of the three resonances are free fit parameters. The mass range covered by the fit was $0.3\ \mathrm{GeV} < m < 2\ \mathrm{GeV}$.

As a cross-check of the reliability of the procedure we performed the fit using another parameterization suggested by A. Minaenko [46]. The $\rho^0(770)$ yield found by this method agrees with our result within 0.5%.

A fit to the distribution of the invariant mass for like sign pairs (Fig. 3) gives a resonance yield at $m_R = 770$ MeV compatible with zero within one standard deviation.

In order to take into account the experimental resolution on the $\pi^+\pi^-$ invariant mass we followed the method described in [9]. We estimated the invariant mass resolution function from the errors on the track parameters in the data as given by the reconstruction program. This function has a FWHM of about 25 MeV and it was convoluted with expression (1) for the fit.

The procedure used to obtain the results presented in Section 6 proceeded through the steps listed below. Steps (i) and (ii) refer to the procedure of obtaining the overall average multiplicities and the resonance widths and masses, while the subsequent steps were made to obtain the differential distributions for the kinematical variables.

(i) Expression (1) is fitted to the raw inclusive experimental distribution.
(ii) The "fully simulated" MC is used to estimate the reconstruction efficiency of various resonances by comparing the yields of reconstructed and generated resonances. The uncorrected yields measured in the data are then divided by these efficiencies.
(iii) A fit to the experimental distributions in each bin of kinematical variables is performed. The reflection normalization factor p and the masses and widths of the resonances are fixed at the values found in step (i).
(iv) Correction factors are obtained in each of the kinematical variable bins similarly to step (ii). The yields of the resonances in each bin are corrected accordingly.
(v) The corrected experimental distributions are plotted and compared with the MC distributions at the event generator level.

The $\bar{\nu}_\mu$ CC sample was treated in the same way, however, due to its lower statistics we limited the analysis to the steps (i) and (ii) and to the $\rho^0(770)$ resonance only.

6. The analysis

6.1. Resonance multiplicities and properties

All the results reported in this section are obtained from the analysis of the ν_μ CC sample.

In Fig. 6 we show the data after subtracting the contribution of the reflections as obtained from the fit. In Fig. 7 we further subtract the contribution of the combinatorial background. The three resonances are clearly visible.

After correcting the result of the fit for the efficiencies as determined from the MC (about 0.77 for all the studied resonances) and for the branching ratios BR($R \to \pi^+\pi^-$) [44] we obtain the results shown in Table 3.

6.2. Resonance multiplicities as a function of the kinematical variables

These results were obtained as described in the Section 5, steps (iii)–(v). For all bins of all kinematical distributions the resonance signals were clearly visible and the value of

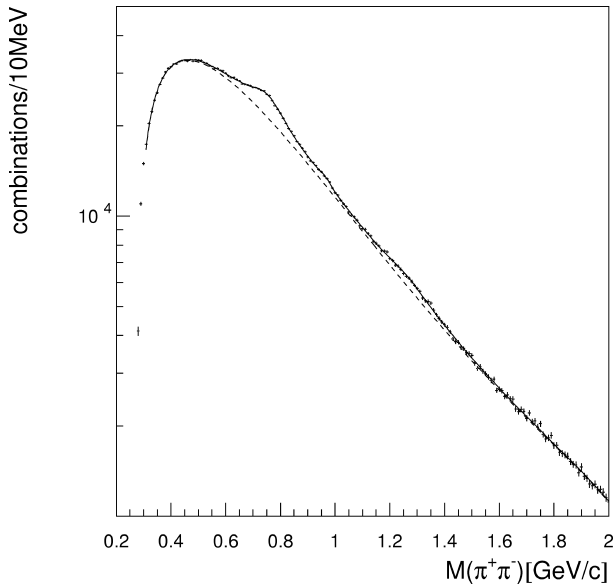

Fig. 6. Distribution of the $\pi^+\pi^-$ invariant mass after subtracting the contribution of reflections.

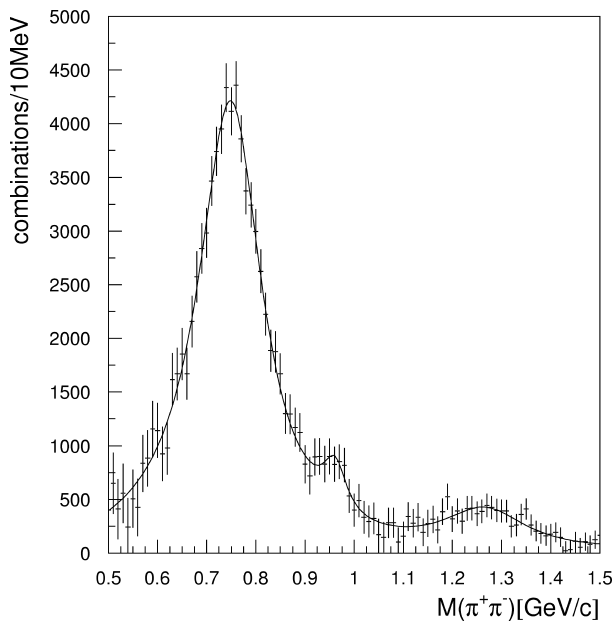

Fig. 7. Distribution of the $\pi^+\pi^-$ invariant mass after subtracting the contributions of both reflections and combinatorial background.

Table 3
Corrected numbers and multiplicities of the three resonances and their measured masses and widths. The errors are statistical only

Resonance	Branching ratio $\pi^+\pi^-$ [44]	Number of resonances	Average multiplicity	Mass (MeV)	Γ (MeV)
$\rho^0(770)$	1.000	130368 ± 4336	0.195 ± 0.007	768 ± 2	151 ± 7
$f_0(980)$	0.666	11809 ± 1965	0.018 ± 0.003	963 ± 5	35 ± 10
$f_2(1270)$	0.564	25189 ± 3958	0.038 ± 0.006	1286 ± 9	198 ± 30

the reduced χ^2 was around 1.0. All the numbers corrected for experimental efficiencies and branching ratios, are compared with the results of the modified Lund simulation (see Section 2.3). The errors shown in the figures are statistical only.

The increase of the average multiplicity of the three resonances as a function of E_ν is shown in Fig. 8.

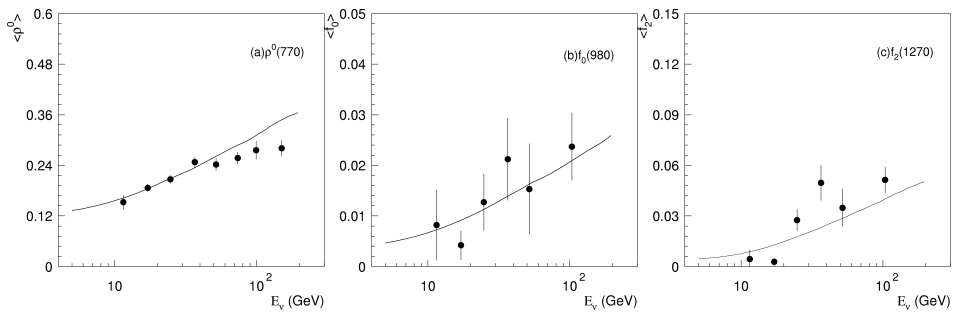

Fig. 8. Average $\rho^0(770)$ (a), $f_0(980)$ (b) and $f_2(1270)$ (c) multiplicity as a function of E_ν. The solid line represents the result of the modified Lund simulation. The errors are statistical only.

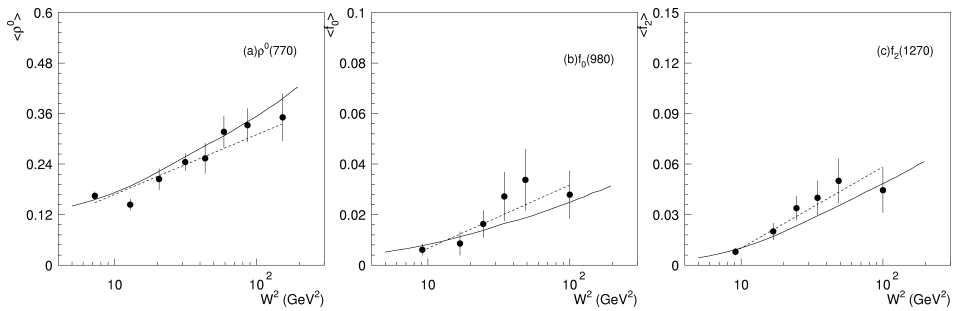

Fig. 9. Average $\rho^0(770)$ (a), $f_0(980)$ (b) and $f_2(1270)$ (c) multiplicity as a function of W^2. The solid line represents the result of the modified Lund simulation. The dashed line represents a fitted function $a + b \ln W^2$. The errors are statistical only.

Table 4
The parameters of the W dependence of the average multiplicities fitted to the expression $a + b \ln W^2$. The errors are statistical only

Resonance	a	b
$\rho^0(770)$	0.026 ± 0.024	0.062 ± 0.009
$f_0(980)$	-0.018 ± 0.008	0.038 ± 0.009
$f_2(1270)$	-0.011 ± 0.003	0.021 ± 0.004

Fig. 9 shows the average multiplicities as a function of W^2. A fit to the average multiplicities with the expression $a + b \ln W^2$ gives the result presented in Table 4 and shown as a dashed line in Fig. 9.

The dependence of the average multiplicities on Q^2 is plotted in Fig. 10.

Fig. 11 shows the x_F dependence of the resonance production. From this picture we see that the forward production of $\rho^0(770)$ and $f_2(1270)$ is enhanced with respect to the backward production. The Lund model overestimates the backward production of these resonances.

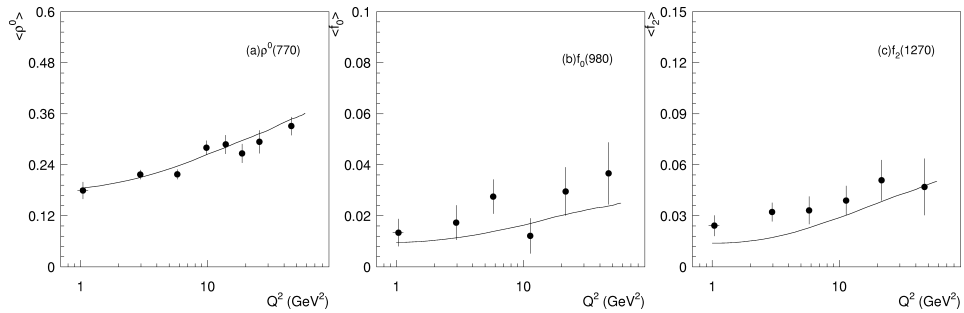

Fig. 10. Average $\rho^0(770)$ (a), $f_0(980)$ (b) and $f_2(1270)$ (c) multiplicity as a function of Q^2. The solid line represents the result of the Lund simulation.

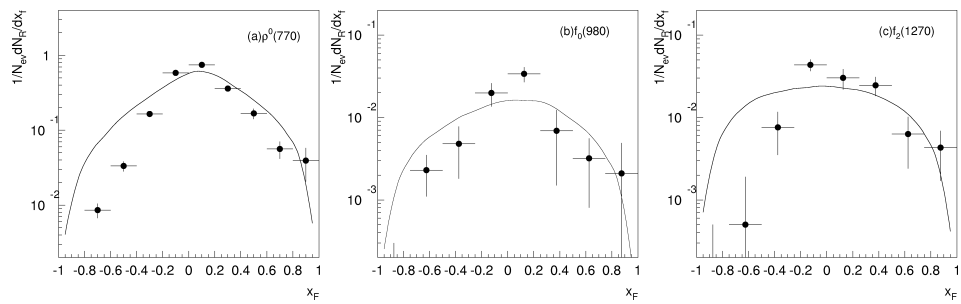

Fig. 11. Average $\rho^0(770)$ (a), $f_0(980)$ (b) and $f_2(1270)$ (c) multiplicity as a function of x_F. The solid line represents the result of the Lund simulation.

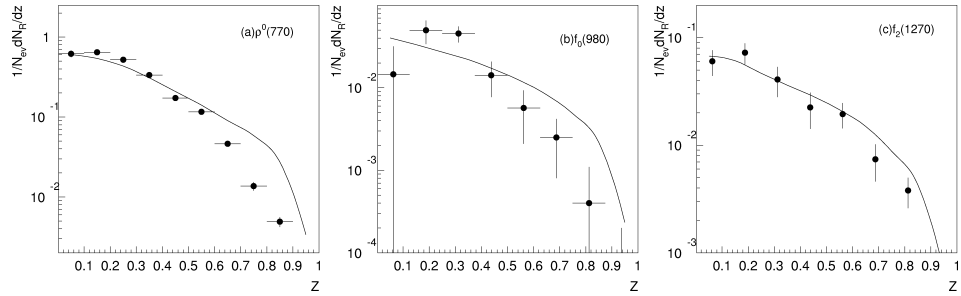

Fig. 12. Average $\rho^0(770)$ (a), $f_0(980)$ (b) and $f_2(1270)$ (c) multiplicity as a function of z (fragmentation functions). The solid line represents the result of the Lund simulation.

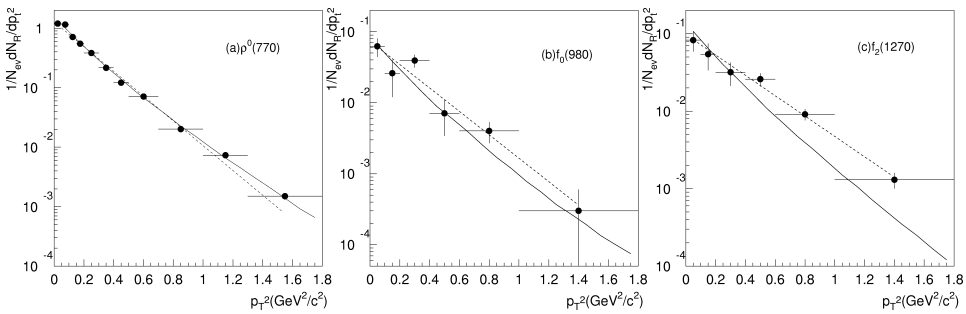

Fig. 13. Average $\rho^0(770)$ (a), $f_0(980)$ (b), and $f_2(1270)$ (c) multiplicity as a function of $p_\perp^2$. The solid line represents the result of the Lund simulation. The dashed straight line represents the result of the fit by the function $ae^{-bp_\perp^2}$.

The resonance fragmentation function is shown in Fig. 12. The high z region of the distributions is overestimated by the Lund model.

The $p_\perp^2$ dependence of the resonance production is shown in Fig. 13. In the case of $\rho^0(770)$ our result favours a steeper $p_\perp^2$ slope than previously measured in [18,20] and agrees with that of Ref. [23]. A fit using the function $ae^{-bp_\perp^2}$ gives

$$a = (1.28 \pm 0.04)\ (\mathrm{GeV}/c)^{-2}, \qquad b = (4.79 \pm 0.07)\ (\mathrm{GeV}/c)^{-2}.$$

An experiment [18] found that the slope parameter b in the range $p_\perp^2 > 0.5\ (\mathrm{GeV}/c)^2$ is different from the slope below this value. We find

$$b = (5.3 \pm 0.2)\ (\mathrm{GeV}/c)^{-2}$$

for $p_\perp^2 < 0.5\ (\mathrm{GeV}/c)^2$, and

$$b = (4.1 \pm 0.1)\ (\mathrm{GeV}/c)^{-2}$$

for $p_\perp^2 > 0.5\ (\mathrm{GeV}/c)^2$. Thus we confirm the existence of two different slopes as found earlier [18].

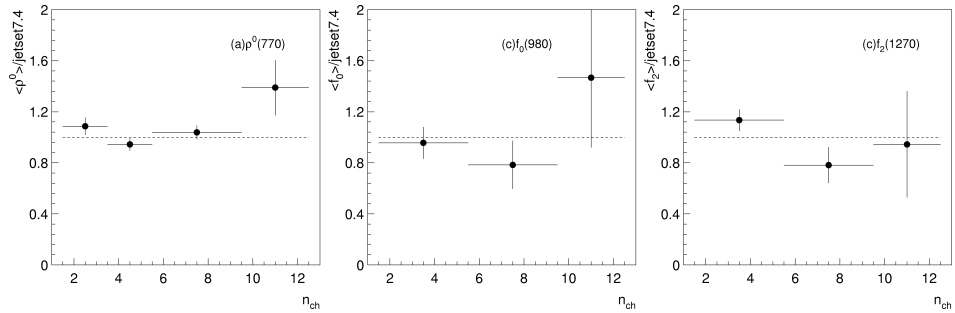

Fig. 14. The resonance multiplicities, normalized to the ones simulated with the Lund model as a function of the hadron jet charged particle multiplicity.

We also observe that the $p_\perp^2$ distribution for $f_2(1270)$ in the data is harder than the results of the Lund model simulation. This could suggest a mass dependence of the $p_\perp^2$ behaviour.

Finally, we address the possibility that the $f_0(980)$ (b) corresponds to the vacuum scalar state suggested by Gribov (see Section 1). Fig. 14 shows the resonance multiplicities divided by the ones simulated with the Lund model as a function of the hadron jet charged track multiplicity. The measured and MC simulated resonance multiplicities were normalized to the same average multiplicity. From Fig. 14 we conclude that in our W range and at our level of accuracy (15–20%) we do not observe the $f_0(980)$ excess at low multiplicities predicted by this model.

7. Systematic uncertainties

The main source of systematic uncertainty results from the subtraction of the reflections. Reflections in the data can be different from the MC not only by a single overall factor but could also have a different shape due to different relative resonance yields. We estimated this effect as follows. The fit to the $\pi^+\pi^-$ invariant mass distribution gave the reflection normalization factor p. We repeated the fit changing p beyond the statistical uncertainty obtained from the initial fit (up to 15%). This results in relative changes of the resonances yields as reported in Table 5.

Other sources of systematics are:

– The uncertainty due to the choice of the fit boundaries: increasing the left boundary by 25 MeV or lowering the right boundary by 300 MeV changes the yields as shown in Table 5.
– Removing the cubic or square term in the exponential function used to describe the background changes the result as shown in the line labelled “Fit model” of Table 5.
– Changing the bin width has a negligible effect on the result.

The overall systematic uncertainty on the measured resonance yields, also shown in Table 5, is obtained by adding all effects in quadrature.

The systematic uncertainties affecting the resonance widths are shown in Table 6.

Table 5
Systematic uncertainties on the resonance yields

Source of systematics	$\rho^0(770)$	$f_0(980)$	$f_2(1270)$
Reflection subtraction	8%	10%	9%
Fit boundaries	4%	8%	9%
Fit model	2%	9%	13%
Total	9%	16%	18%

Table 6
Systematic uncertainties on the resonance widths, in MeV

Source of systematics	$\rho^0(770)$	$f_0(980)$	$f_2(1270)$
Reflection subtraction	13	3	11
Bin width	5	3	1
Fit model	12	5	6
Total	18	7	13

Table 7
Total corrected numbers and yields of resonances and their masses and widths. The errors include statistical and systematic error

Resonance	Number of resonances	Average multiplicity	Mass (MeV)	Γ (MeV)
$\rho^0(770)$	130368 ± 12509	0.195 ± 0.019	768 ± 2.5	151 ± 19
$f_0(980)$	11809 ± 2726	0.018 ± 0.004	963 ± 5	35 ± 12
$f_2(1270)$	25189 ± 6018	0.038 ± 0.009	1286 ± 11	198 ± 32

Table 7 summarizes our results with statistical and systematic uncertainties added in quadrature.

8. Yields of $\rho^0(770)$ and comparison with previous experiments

The average $\rho^0(770)$ multiplicity measured in the NOMAD experiment for neutrino and antineutrino charged current interactions is shown in Table 8, together with the results from previous experiments. In the neutrino charged current sample, our measurement confirms the results of all previous experiments in a similar W range with a much better statistical accuracy. The deviation of the SKAT [24] result is usually explained as due to the lower average W. In the case of $\bar{\nu}_\mu$, there was some disagreement between previous experiments which could not be explained by different W ranges. Our result confirms the measurements in which the average $\rho^0(770)$ multiplicity in $\bar{\nu}_\mu$ CC interactions is the same as in ν_μ CC interactions.

Table 8
Average $\rho^0(770)$ multiplicity in ν_μ and $\bar{\nu}_\mu$ experiments

Reaction	W	Average multiplicity	Reference
ν_μ nucleon	$W > 2$ GeV	$0.195 \pm 0.007 \pm 0.019$	this analysis
ν_μp	5.5	$0.18 \pm 0.02 \pm 0.02$	[18]
ν_μp	$W > 2$ GeV	$0.21 \pm 0.03 \pm 0.03$	[23]
ν_μp	4.9	0.16 ± 0.02	[21]
ν_μp	$W > 2$ GeV	0.20 ± 0.05	[28]
ν_μp	5.0	0.21 ± 0.04	[25]
ν_μn	$W > 2$ GeV	$0.21 \pm 0.02 \pm 0.03$	[23]
ν_μn	–	0.17 ± 0.05	[28]
ν_μNe	4.8	0.17 ± 0.04	[19]
ν_μ freon	3.1	0.09 ± 0.02	[24]
$\bar{\nu}_\mu$ nucleon	$W > 2$ GeV	$0.18 \pm 0.02 \pm 0.02$	this analysis
$\bar{\nu}_\mu$p	4.4	$0.12 \pm 0.02 \pm 0.02$	[18]
$\bar{\nu}_\mu$p	$W > 2$ GeV	$0.20 \pm 0.02 \pm 0.03$	[23]
$\bar{\nu}_\mu$p	4.2	0.11 ± 0.02	[22]
$\bar{\nu}_\mu$p	3.4	0.21 ± 0.03	[26]
$\bar{\nu}_\mu$n	$W > 2$ GeV	$0.18 \pm 0.03 \pm 0.03$	[23]
$\bar{\nu}_\mu$Ne	3.9	0.12 ± 0.02	[20]
$\bar{\nu}_\mu$Ne	4.3	0.13 ± 0.02	[27]

9. Conclusions

The inclusive production of the meson resonance $\rho^0(770)$ in neutrino–nucleon charged current interactions has been studied with much better statistical accuracy than in previous experiments.

We also looked for other resonances decaying to $\pi^+\pi^-$ pairs. For the first time the $f_0(980)$ meson is observed in neutrino interactions. The signal has a significance of about 5 standard deviations.

We see a clear signal of $f_2(1270)$. Its production in neutrino interactions is reliably established.

A global fit to the $\pi^+\pi^-$ pair mass distribution allows us to obtain the masses and the widths of the $\rho^0(770)$, $f_0(980)$ and $f_2(1270)$.

The average multiplicities of $\rho^0(770)$, $f_0(980)$ and $f_2(1270)$ are measured as a function of W^2, Q^2 and other kinematic variables. These results are compared with a simulation based on a modified Lund model. Good agreement for most of the distributions is found.

In addition, the production of $\rho^0(770)$ in $\bar{\nu}_\mu$ CC interactions has been studied with lower statistics. This allowed us to clarify the ambiguous experimental situation on the production of $\rho^0(770)$ in antineutrino interactions.

We see no evidence of the enhanced $f_0(980)$ production in low multiplicity events predicted by Gribov et al. [14,15].

These studies demonstrate the capability of NOMAD to obtain results which up to now have been the exclusive domain of bubble-chamber experiments, but with much improved statistics.

Acknowledgements

We gratefully acknowledge the CERN SPS accelerator and beam-line staff for the magnificent performance of the neutrino beam. The experiment was supported by the following funding agencies: Australian Research Council (ARC) and Department of Industry, Science, and Resources (DISR), Australia; Institut National de Physique Nucléaire et Physique des Particules (IN2P3), Commissariat à l'Energie Atomique (CEA), France; Bundesministerium für Bildung und Forschung (BMBF, contract 05 6DO52), Germany; Istituto Nazionale di Fisica Nucleare (INFN), Italy; Joint Institute for Nuclear Research and Institute for Nuclear Research of the Russian Academy of Sciences, Russia; Fonds National Suisse de la Recherche Scientifique, Switzerland; Department of Energy, National Science Foundation (grant PHY-9526278), the Sloan and the Cottrell Foundations, USA.

We are grateful to V.A. Uvarov, A.A. Minaenko, V.G. Zaec for the discussions of models and fit methods.

References

[1] B. Andersson et al., Phys. Rep. 97 (1983) 31.
[2] G.C. Fox, S. Wolfram, Nucl. Phys. B 168 (1980) 285.
[3] DELPHI Collaboration, P. Abreu et al., Phys. Lett. B 449 (1999) 364.
[4] OPAL Collaboration, K. Ackerstaff et al., Eur. Phys. J. C 4 (1998) 19;
OPAL Collaboration, K. Ackerstaff et al., Eur. Phys. J. C 5 (1998) 441.
[5] ALEPH Collaboration, D. Buskulic et al., Z. Phys. C 69 (1996) 393.
[6] ARGUS Collaboration, H. Albrecht et al., Z. Phys. C 61 (1994) 1.
[7] TASSO Collaboration, R. Braunschweig et al., Z. Phys. C 47 (1990) 167.
[8] CELLO Collaboration, H.J. Behrend et al., Z. Phys. C 46 (1990) 397.
[9] OMEGA Collaboration, R.J. Apsimon et al., Z. Phys. C 53 (1992) 581;
OMEGA Collaboration, R.J. Apsimon et al., Z. Phys. C 56 (1992) 185.
[10] G. Eszes et al., Acta Phys. Hung. 64 (1989) 177;
M. Arneodo et al., Z. Phys. C 33 (1986) 167.
[11] NA22 Collaboration, N.M. Agababyan et al., Z. Phys. C 46 (1990) 387;
NA27 Collaboration, M. Aguilar-Benites et al., Z. Phys. C 50 (1991) 407;
M. Deutschmann et al., Nucl. Phys. B 103 (1976) 426.
[12] R.L. Jaffe, K. Johnson, Phys. Lett. B 60 (1976) 201;
R.L. Jaffe, Phys. Rev. D 15 (1977) 267;
R.L. Jaffe, Phys. Rev. D 15 (1977) 269.
[13] J. Weinstein, N. Isgur, Phys. Rev. D 41 (1990) 2236.
[14] V.N. Gribov, Lund preprint, LU-TP 91-7.
[15] F.E. Close et al., Phys. Lett. B 319 (1993) 291.
[16] D. Robson, Nucl. Phys. B 130 (1977) 328.

[17] F.E. Close, Phys. Lett. B 397 (1997) 333;
A. Kirk, Yad. Fiz. 62 (1999) 439.
[18] G.T. Jones et al., Z. Phys. C 51 (1991) 11.
[19] G.T. Jones et al., Z. Phys. C 51 (1991) 205.
[20] W. Wittek et al., Z. Phys. C 44 (1989) 175.
[21] P. Allen et al., Nucl. Phys. B 194 (1982) 373.
[22] H. Grassler et al., Nucl. Phys. B 272 (1986) 253.
[23] D. Allasia et al., Nucl. Phys. B 268 (1986) 1.
[24] V.V. Ammosov et al., Sov. J. Nucl. Phys. 46 (1987) 80.
[25] J. Berge et al., Phys. Rev. D 22 (1980) 1043.
[26] M. Derrick et al., Phys. Lett. B 91 (1980) 307.
[27] V.V. Ammosov et al., Sov. J. Nucl. Phys. 45 (1987) 457.
[28] C.C. Chang et al., in: Proc. 1981 Int. Conf. on Neutrino Physics and Astrophysics, Maui, Hawaii, Vol. 2, 1981, p. 162.
[29] V.V. Ammosov et al., Sov. J. Nucl. Phys. 46 (1987) 998;
V.V. Ammosov et al., J. Phys. Soc. Jap. 55 suppl. (1986) 984.
[30] W. Wittek et al., Phys. Lett. B 187 (1987) 179.
[31] V.G. Zaetz et al., Z. Phys. C 66 (1995) 583.
[32] J. Altegoer et al., NOMAD Collaboration, Nucl. Instrum. Methods A 404 (1998) 96.
[33] M. Anfreville et al., The drift chambers of the NOMAD detector, to be submitted to Nucl. Instrum. Methods.
[34] G. Bassompierre et al., Nucl. Instrum. Methods A 403 (1998) 363;
G. Bassompierre et al., Nucl. Instrum. Methods A 411 (1998) 63.
[35] D. Autiero et al., Nucl. Instrum. Methods A 372 (1996) 556;
D. Autiero et al., Nucl. Instrum. Methods A 373 (1996) 358;
D. Autiero et al., Nucl. Instrum. Methods A 387 (1997) 352;
D. Autiero et al., Nucl. Instrum. Methods A 411 (1998) 285.
[36] J. Altegoer et al., Nucl. Instrum. Methods A 428 (1999) 299.
[37] G. Acquistapace et al., CERN-ECP/95-14, July 1995.
[38] G. Collazuol et al., Nucl. Instrum. Methods A 449 (2000) 609.
[39] G. Ingelman, A. Edin, J. Rathsman, Lepto 6, Program Manual, DESY 96-057.
[40] T. Sjostrand, Comput. Phys. Commun. 82 (1994) 74.
[41] GEANT: Detector description and simulation tool, CERN Programming Library Long Writeup W5013.
[42] G.T. Jones et al., Z. Phys. C 25 (1984) 121;
G.T. Jones et al., Z. Phys. C 27 (1985) 43;
H. Graessler et al., Nucl. Phys. B 223 (1983) 269.
[43] V.V. Ammosov et al., Sov. J. Nucl. Phys. 43 (1986) 1186.
[44] Particle Data Group, D.E. Groom et al., Eur. Phys. J. C 15 (2000) 1.
[45] J.D. Jackson, Nuovo Cimento 34 (1964) 1644;
J.D. Jackson, Eur. Phys. J. C 15 (2000) 1.
[46] A.A. Minaenko et al., Z. Phys. C 62 (1994) 15.